Papers in Physics, vol. 14, art. 140002 (2022)

www.papersinphysics.org

Received: 10 October 2021, Accepted: 21 December 2021
Edited by: O. Martínez
Reviewed by: A. M. Llois - Universidad de Buenos Aires, Argentina

DOI: http://doi.org/10.4279/PIP.140002

ISSN 1852-4249

Electronic and optical properties of nickel-doped ceria: A computational modelling study

Hussein A. Miran[1*], Zainab N. Jaf[1]

Cerium oxide (CeO_2), or ceria, has gained increasing interest owing to its excellent catalytic applications. Under the framework of density functional theory (DFT), this contribution demonstrates the effect that introducing the element nickel (Ni) into the ceria lattice has on its electronic, structural, and optical characteristics. Electronic density of states (DOSs) analysis shows that Ni integration leads to a shrinkage of Ce $4f$ states and improvement of Ni $3d$ states in the bottom of the conduction band. Furthermore, the calculated optical absorption spectra of an Ni-doped CeO_2 system shifts towards longer visible light and infrared regions. Results indicate that Ni-doping a CeO_2 system would result in a decrease of the band gap. Finally, Mulliken's charge transfer of the $Ce_{1-x}Ni_xO_2$ system exhibits an ionic bond between Ce or Ni and O, and covalent bonds between Ce and Ni atoms. The analysis of absorption spectra demonstrates that Ni-doped CeO_2 is a material with potential use in photocatalytic, photovoltaic, and solar panels.

I. Introduction

Cerium oxide (ceria or CeO_2) based materials have generated extensive interest due to their exceptional electronic, optical, magnetic, and mechanical properties. Ceria is used in a broad array of applications such as catalysts [1, 2], photocatalysts, optoelectronics and opto-magnetic devices [3, 4]. One of the features that renders ceria useful for catalysis is its ability to release or uptake oxygen from its lattice without substantial structural re-arrangement or the loss of its fluorite lattice [5, 6]. In the fluorite structure, Ce atoms demonstrate a change in oxidation state from Ce^{4+} to Ce^{3+} and increase the tendency for redox [7]. Nickel-based compounds, on the other hand, are being revealed to have fundamental and technological applications [8–10]. It has been reported that the introduction of dopants into ceria can facilitate band gap reduction, which in turn leads to the extension of light absorption into the visible range of electromagnetic radiation. Corma *et al.* [11] suggested that non-dye-sensitized solar cells with suitable dopant levels may deliver a new group of effective solar cells that, without photosensitization, have photovoltaic behaviour in the visible range. Qi-Ye proposed that, while pure CeO_2exhibits a trivial dielectric constant of 4, inserting a small amount of Fe (0.9 at. %) promotes densification and results in a larger dielectric constant of 23. Furthermore, the absorption coefficient of Fe-doped CeO_2at frequencies extending from 0.2 to 1.8 THz is less than 0.35 cm^{-1}, suggesting that Fe-doped $CeO_2$is a probable terahertz (THz) optical substance [12]. Moreover, Xia *et al.* [13] have fabricated Mn-modified CeO_2 nanorods and reported that the peak of the absorption spectrum of CeO_2 shifts from ultraviolet into the region of visible light after Mn insertion. Likewise, photolu-

*hussein.a.j@ihcoedu.uobaghdad.edu.iq

[1] Department of Physics, College of Education for Pure Sciences / Ibn-Al-Haitham, University of Baghdad, Baghdad, Iraq.

minescence spectra analysis of Ni-doped CeO_2 films demonstrates that oxygen vacancies are formed upon Ni-doping of CeO_2. The shift in the UV peak indicates that Ni-doping can notably tailor the electronic structure and band gap of CeO_2. Tiwari *et al.* [14] reported the synthesis of $Ce_{1-x}Ni_xO_2$ (0 x 0.1) nanopowders. UV-visible analysis suggests a reduction of band gap upon incorporation of Ni atoms into the host lattice. They attributed the decrease in band gap to the augmented disorder caused by defect formations between valance and conduction bands. Another study reported the impact of Mg inclusion on optical performance of CeO_2 nanowires. They concluded from the absorption spectra that band gap energy is minimized to 3.00 eV when incorporating Mg ions [15]. Fe-doped CeO_2 enhanced photocatalytic activity towards the degradation of Methyl Orange (MO) [16]. The inclusion of Fe and Ni ions into the crystal lattice of CeO_2 nanoparticles significantly reduces the dielectric constant value of the pure CeO_2 [17]. Literature regarding density functional theory (DFT) has revealed that inclusion of Ni into the CeO_2 lattice would improve the catalytic and optical properties of the resulting system [18]. Likewise, we have theoretically confirmed that Titanium (Ti) doped ceria promotes a band gap reduction which in turn leads the modified system to be useful in optical and catalytic applications [19]. To this end, and motivated by the above-mentioned literature, this contribution demonstrates the theoretical prospect of Ni-substituted CeO_2, aiming to gain insight into the electronic, structural, and optical properties of the adapted configurations.

II. Methodology

The computational modeling in this investigation was performed using the Cambridge Serial Total Energy Package (CASTEP) under the frame of density functional theory (DFT) [20]. The bare DFT was reported to undervalue the energy of the electronic band gap because of the robust Coulomb interaction between the electrons in the Ce $4f$ state [21]. Therefore, the Hubbard factor (U) has been added to the DFT functional (GGA) in the form of (GGA+U), by which all the simulated findings were computed [22]. The DFT+U approach has previously been utilized to investigate thermodynamic stability of $CoCu_2O_3$ surfaces [23]. Additionally, according to the suggested values of the default CASTEP settings, the U values were fixed at 6.0 eV for Ce and 2.5 eV for Ni. Ultrasoft pseudopotentials were utilized to describe the interaction between electrons and ions in reciprocal space with valence electron arrangements of $2s^2\ 2p^4$ for O, $3d^8\ 4s^2$ for Ni, and $4f^1\ 5s^2\ 5p^6\ 5d^1\ 6s^2$ for Ce. To set the Ni-doped concentrations, the substitution systems were built at $x = 0.25$, and 0.50, suggesting that at $x = 0.25$, only one Ce atom has been replaced by Ni, whereas for $x = 0.50$, two vacant Ce atoms are occupied by Ni. In a similar approach, the $Ce_{1-x}Ni_xO_2$ systems correspond to Ni concentrations of $x = 0.25$ and 0.50, as depicted in Fig. 1. In order to minimize the total energy of $Ce_{1-x}Ni_xO_2$ structures, a cut off energy of 300 eV was set along with a Monkhorst-Pack grid of $3 \times 2 \times 2$ k-points in the Brillouin zone. The energy convergence tolerance was fixed at 5.0×10^{-6} eV/atom. For the geometry optimization process of the investigated structures, the maximum displacement tolerances, maximum stress, maximum force and energy change were set at 0.001Å, 0.05 GPa, 0.03 eV/Å and 1×10^{-6} eV/atom, respectively. Electronic properties such as total and partial density of states and the Mulliken bond population, as well as optical properties, were directly computed by CASTEP. Lastly, to reproduce the exact electronic band gap energy of CeO_2, a scissor operator of 1 eV was applied and employed for all the following optical calculations.

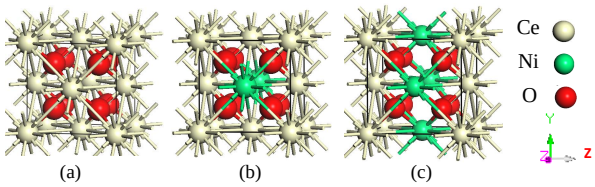

Figure 1: The optimized unit cell structures of $Ce_{1-x}Ni_xO_2$ systems as plotted by VESTA visualization software at (a) $x = 0$, (b) $x = 0.25$, (c) $x = 0.50$. White spheres represent Ce atoms; light green spheres denote Ni atoms, and O atoms are indicated by red spheres.

Table 1: The calculated lattice constants (Å), band gap energy (eV), and charge distribution (e) for bare and Ni-modified CeO_2 structures.

Geometry	Lattice parameter (Å)	Formation Energy (eV)	Band gap energy (eV)	Charge distribution (e)		
				Ce	Ni	O
CeO_2	$a = 5.46$	—	3.19	1.30	—	−0.65
$Ce_{0.75}Ni_{0.25}O_2$	$a = 5.36$	−7.94	1.75	1.34	0.27	−0.59
$Ce_{0.50}Ni_{0.50}O_2$	$a = 5.22$	−7.10	1.55	1.43	0.71	−0.53

III. Results and discussion

i. Geometrical relaxation

The relaxed configurations of bare and Ni-doped CeO_2 are displayed in Fig. 1. Typically, CeO_2 adopts a cubic fluorite-type structure with a space group of (Fm-3m). The number of formula units in the unit cell corresponds to four (i.e. 4 cerium atoms and 8 oxygen atoms). The calculated lattice constants confirmed the experimental amount of a = 5.410 Å [24], and these constants, along with the Mulliken population findings of the relaxed structures, are presented in Table 1. The atomic radius of Ce is larger than the atomic radius of Ni, which correspond to 2.7 Å and 1.62 Å, respectively. Therefore, a reduction in the lattice constants can be observed when Ni contents increase, suggesting a lattice alteration by the insertiion of Ni ions. To assess the stability of the chosen doped matrix along with the difficulty of Ni-doping such a system, the doping formation energy (E_f) has been computed for the systems via the following relationship [25]:

$$E_{f_{\mathrm{Ce}_k\mathrm{Ni}_l\mathrm{O}_m}} = \frac{E_{\mathrm{Ce}_k\mathrm{Ni}_l\mathrm{O}_m} - kE_{\mathrm{Ce}} - lE_{\mathrm{Ni}} - mE_{\mathrm{O}}}{k+l+m}, \quad (1)$$

wherein the parameters k, l and m, refer to the molar fractions of elements Ce, Ni, and O in the alloyed systems.

The negative values of doping formation energy depicted in Table 1 indicate that the selected structures are stable and some amount of energy is released with the introduction of Ni atoms into the host system. Regarding the comparison between the current system and the system studied in Ref. [19], both systems are stable since the formation energies reveal negative values. Table 1 reports Mulliken's charge populations of Ce, O and Ni atoms in the $Ce_{1-x}Ni_xO_2$ system. As the table shows, Ce and Ni atoms in the studied structures tend toward positive charges whereas O atoms are linked to negative charges.

The simulation results of Mulliken's charge values also indicate a covalent behaviour for the Ni-Ce bond in the designated structures that comprise Ni and Ce atoms, and ionic properties for Ni-O

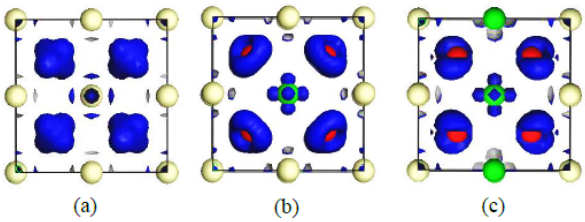

Figure 2: The calculated electron density difference for the studied systems. (a), (b), (c) corresponding to CeO_2, $Ce_{1-x}Ni_xO_2$ ($x = 0.25$), $Ce_{1-x}Ni_xO_2$ ($x = 0.50$), respectively.

Table 2: The interatomic distances (Å) and angles (°) between the selected atoms of the studied systems.

Geometry	Interatomic distances (Å)		Angles (°)	
CeO_2	Ce-O	2.36	O-Ce-O	70.52
	O-O	2.73		
$Ce_{0.75}Ni_{0.25}O_2$	Ni-O	2.26	O-Ni-O	69.97
	Ce-O	2.31	O-Ce-O	69.83
	O-O	2.61	Ni-O-Ce	110.88
$Ce_{0.50}Ni_{0.50}O_2$	Ni-O	2.19	O-Ni-O	64.98
	Ce-O	2.32	O-Ce-O	68.42
	O-O	2.59	Ni-O-Ce	109.01

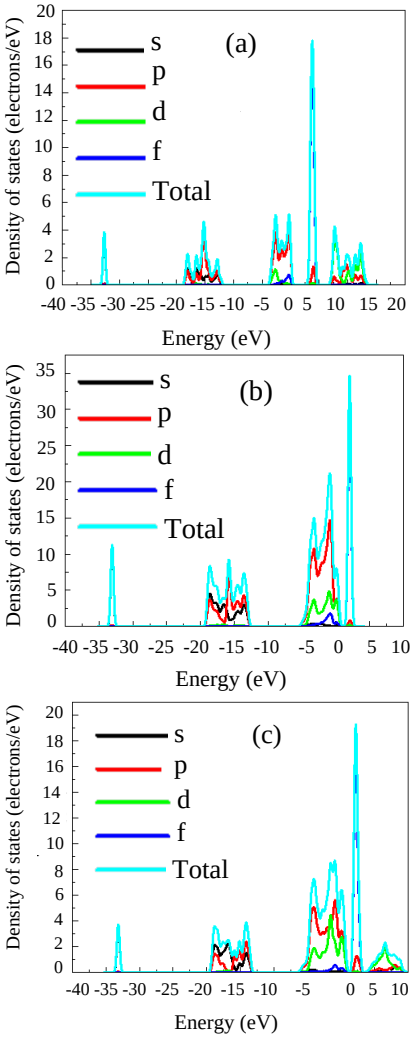

Figure 3: The total density of states (TDOSs) and partial density of states (PDOSs) of $Ce_{1-x}Ni_xO_2$ unit cell versus the energy of electrmagnetic wave at (a) $x = 0$, (b) $x = 0.25$, (c) $x = 0.50$.

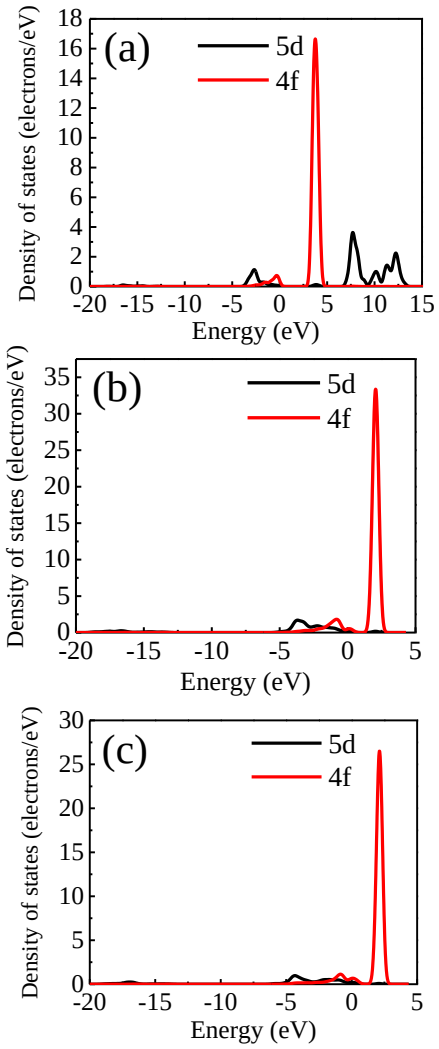

Figure 4: $5d$ and $4f$ orbitals of Ce atom in $Ce_{1-x}Ni_xO_2$, (a) $x = 0$, (b) $x = 0.25$, (c) $x = 0.50$.

and Ce-O bonds. Furthermore, the findings show that Ce atoms lose more electrons once Ni is implanted into the host lattice, whereas the increase in O atoms' electrons is approximately constant as Ni contents increase [26]. Figure 2 displays the distribution of the charge density, and the blue colour around the O atoms demonstrates the electron density gain resulted from inserting Ni atoms.

Furthermore, Table 2 demonstrates the calculated interatomic bonds and angles between select atoms of the optimized structures. The findings indicate a reduction in the bonds and angles of the doped systems as compared to the host CeO_2 lattice.

ii. Electronic properties analysis

The electronic properties of the $Ce_{1-x}Ni_xO_2$ system can be investigated by studying the density of states (DOSs) of the relaxed geometries. Results of DOSs are plotted and shown in Fig. 3. CeO_2 demonstrates non-metallic behaviour, indicating

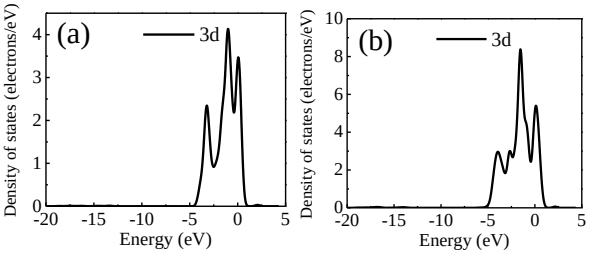

Figure 5: $3d$ orbitals of Ni atom loadings in $Ce_{1-x}Ni_xO_2$ system. (a) $x = 0.25$, (b) $x = 0.50$.

a semiconducting nature. The Fermi level is situated at zero energy in order to clearly identify the band gap energy. Regarding the bare CeO_2 unit cell, the DOSs plotted correspond well with the results of previously published studies [27]. The uppermost valance band is extended from -3.7 to 0 eV (Fermi level), while the conduction band is located at 3.19 eV above the Fermi level. This finding signifies the possibility of reproducing the experimentally assessed band gap energy of [28] 3.19 as portrayed in Fig. 3(a). Moreover, Ni-doped ceria at various contents (0.25 and 0.50) involve high intensity states in the conduction and valence bands. On the other hand, band gap energy is minimized to 1.75 eV and 1.55 eV at Ni concentrations of 0.25

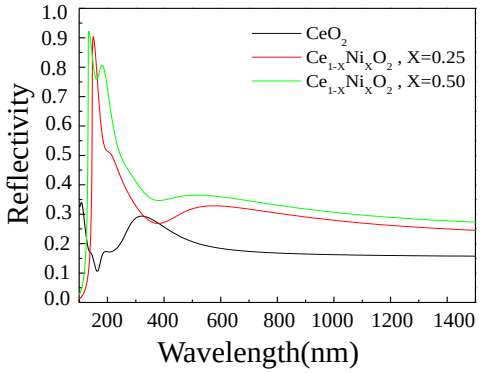

Figure 6: Reflectance spectra of pure CeO_2 and Ni-doped CeO_2 configurations. As Fig. 6 shows, spectra representing Ni-added CeO_2 reveal high reflectivity values in the ultra-violet region when compared to the pure ceria reflectivity spectrum. Further, all the spectra demonstrate a moderate trend to reflect incident photons within the visible range [29].

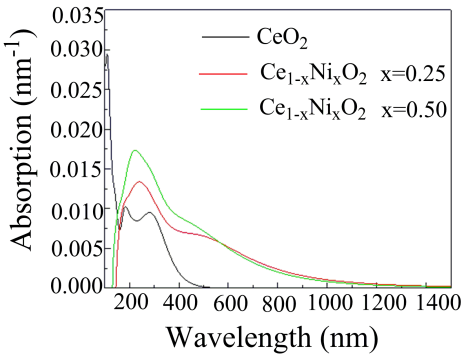

Figure 7: The calculated absorption spectra for bare and Ni-doped CeO_2 configurations.

and 0.50, correspondingly, thus demonstrating that Ni integration into ceria would minimize the band gap energy. Figure 4 shows DOS plots of $5d$ and $4f$ states of Ce atom in pure and doped $Ce_{1-x}Ni_xO_2$. As seen from the figure, $4f$ states in the conduction band shift toward the Fermi level as the Ni concentration increases, resulting in a reduction of the electronic band gap.

Furthermore, comparing the Ni $3d$ states in the $Ce_{1-x}Ni_xO_2$ ($x = 0.25$) with ($x = 0.50$) structures (depicted in Fig.5), it is observed that the Ni $3d$ states are positioned at the same energy level, signifying that the Ni $3d$ states would improve with rising Ni contents. Additionally, further reduction in the band gap energy with the introduction of Ni can be possibly ascribed to the accumulation of Ni $3d$ states in the conduction band, leading to improved photocatalytic and optical performance of $Ce_{1-x}Ni_xO_2$.

iii. Optical properties

The reflectivity of pure and Ni-doped CeO_2 in terms of wavelength is shown in Fig. 6. As demonstrated, spectra represented by Ni-added CeO_2 reveal high reflectivity values in the ultra-violet region when compared to the reflectivity spectrum of pure ceria. Furthermore, all the spectra demonstrate a moderate trend to reflect incident photons within the visible range [29].

Absorption coefficients specify how far light of a certain energy or wavelength is able to enter a substance before absorption. The absorption spectra of the studied structures are shown in Fig. 7

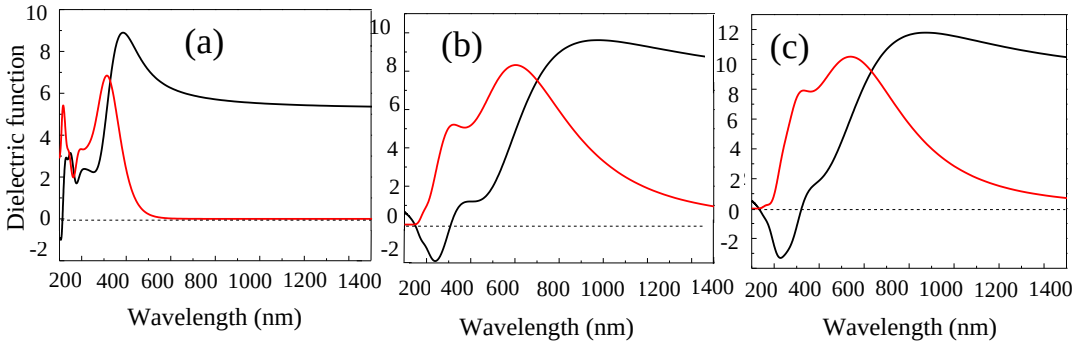

Figure 8: The real and imaginary components of dielectric function of $Ce_{1-x}Ni_xO_2$ at (a) $x = 0$; (b) $x = 0.25$; (c) $x = 0.50$. Black and red curves represent the real and imaginary parts, respectively.

and demonstrate a semiconductive character because the spectra originate at non-zero values of wavelength.

It is well known that the dielectric function is an important factor related to the absorption and polarization properties of materials. The examined dielectric constant of undoped and Ni-doped CeO_2 are depicted in Fig. 8. The non-zero values of the imaginary component of the dielectric constant indicate the process of absorption in that energy region.

IV. Conclusions

The current study demonstrates the influence of Ni addition on the electronic, structural and optical properties of CeO_2. The attained outcomes recommend that addition of Ni into ceria would reduce the band gap to 1.75 eV and 1.55 eV at 0.25 and 0.50, respectively. Moreover, Ni-doping introduces $3d$ states in the conduction band of CeO_2. The $3d$ states have a significant effect on dropping the band gap energy. Furthermore, the absorption spectra of CeO_2 is shifted from ultraviolet towards the visible ranges after Ni incorporation. This implies that optical absorption is elongated to a longer wavelength region. Mulliken's charge distribution displayed an ionic behaviour for Ce-O and Ni-O bonds, whereas Ce-Ni bonds exhibited a covalent behaviour. Results from this study demonstrate that Ni-doped CeO_2 is a potential candidate in photocatalytic and optical applications.

[1] C Riley, A De La Riva, *et al.* , *Synthesis of nickel-doped ceria catalysts for selective acetylene hydrogenation*, ChemCatChem **11**, 1526 (2019).

[2] H A Miran, M Altarawneh, Z T Jiang, H Oskierski, M Almatarneh, B Z Dlugogorski, *Decomposition of selected chlorinated volatile organic compounds by ceria (CeO_2)*, Catal. Sci. Technol. **7**, 3902 (2017).

[3] Z G Yan, C H Yan, *Controlled synthesis of rare earth nanostructures*, J. Mater. Chem. **18**, 5046 (2008).

[4] K R B Singh, V Nayak, T Sarkar, R P Singh, *Cerium oxide nanoparticles: Properties, biosynthesis and biomedical application*, RSC Adv. **10**, 27194 (2020).

[5] H A Miran, Z N Jaf, M Altarawneh, Z-T Jiang, *An insight into geometries and catalytic applications of CeO_2 from a DFT outlook*, Molecules **26**, 6485 (2021).

[6] T Naganuma, E Traversa, *Stability of the Ce3+ valence state in cerium oxide nanoparticle layers*, Nanoscale **4**, 4950 (2012).

[7] H A Miran, M Altarawneh, *et al.*, *Thermomechanical properties of cubic lanthanide oxides*, Thin Solid Films **653**, 37 (2018).

[8] R Paulose, R Mohan, V Parihar, *Nanostructured nickel oxide and its electrochemical behaviour A brief review*, Nano-Structures & Nano-Objects **11**, 102 (2017).

[9] M F Altaee, L A Yaaqoob, Z K Kamona, *Evaluation of the biological activity of nickel oxide nanoparticles as antibacterial and anticancer agents*, Iraqi J. Sci. **61**, 2888 (2020).

[10] A S Mohammed, I M Ibrahim, A Ramizy, *Energy band diagram of NiO: Lu_2O_3/n-Si heterojunction*, Iraqi J. Sci. **59**, 287 (2018).

[11] A Corma, P Atienzar, H García, J Y Chane-Ching, *Hierarchically mesostructured doped CeO_2 with potential for solar-cell use*, Nat. Mater. **3**, 394 (2004).

[12] Q Y Wen, H W Zhang, Q H Yang, S Li, D G Xu, J Q Yao, *Fe-Doped polycrystalline CeO_2 as terahertz optical material*, Chinese Phys. Lett. **26**, 047803 (2009).

[13] C Xia, C Hu, P Chen, B Wan, X He, Y Tian, *Magnetic properties and photoabsorption of the Mn-doped CeO_2 nanorods*, Mater. Res. Bull. **45**, 794 (2010).

[14] S Tiwari, G Rathore, *et al.*, *Oxygen and cerium defects mediated changes in structural, optical and photoluminescence properties of Ni substituted CeO_2*, J. Alloys Compd. **782**, 689 (2019).

[15] X Ma, P Lu, P Wu, *Structural, optical and magnetic properties of CeO_2 nanowires with nonmagnetic Mg2+ doping*, J. Alloys Compd. **734**, 22 (2018).

[16] D Channei, B Inceesungvorn, N Wetchakun, S Ukritnukun, A Nattestad, J Chen, S Phanichphant, *Photocatalytic degradation of methyl orange by CeO_2 and Fe-doped CeO_2 films under visible light irradiation* Sci. Rep. **4**, 1 (2014).

[17] R Zamiri, S A Salehizadeh, H A Ahangar, M Shabani, A Rebelo, J M F Ferreira, *Dielectric and optical properties of Ni- and Fe-doped CeO_2 nanoparticles*, Appl. Phys. A-Mater. **125**, 1 (2019).

[18] D Rajsfus, A Salcedo, B Milberg, B Irigoyen, *Nickel deposition on ceria: A DFT+U study*, An. Asoc. Quim. Argent. **104**, 44 (2017).

[19] H A Miran, Z N Jaf, I H Khaleel, A A Alkhafaji, *Photocatalytic and optical performances of CeO_2 by substitution of titanium*, Phys. Chem. Res. **9**, 553 (2021).

[20] M D Segall, P J D Lindan, M J Probert, C J Pickard, P J Hasnip, S J Clark, M C Payne, *First-principles simulation: Ideas, illustrations and the CASTEP Code*, J. Phys. Condens. Matter **14**, 2717 (2002).

[21] A J Cohen, P Mori-Sánchez, W Yang, *Insights into current limitations of density functional theory*, Science **321**, 792 (2008).

[22] H A Miran, M Altarawneh, Z N Jaf, M M Rahman, M H Almatarneh, Z T Jiang, *Influence of the variation in the Hubbard parameter (U) on activation energies of CeO_2-catalysed reactions*, Can. J. Phys. **98**, 385 (2020).

[23] H Widjaja, H A Miran, M Altarawneh, I Oluwoye, H N Lim, N M Huang, Z T Jiang, B Z Dlugogorski, *DFT+ U and ab initio atomistic thermodynamics approache for mixed transitional metallic oxides: A case study of $CoCu_2O_3$ surface terminations*, Mater. Chem. Phys. **201**, 241 (2017).

[24] Y Xue, D Tian, D Zhang, C Zeng, Y Fu, K Li, H Wang, Y Tian, *The mechanism of photocatalyst and the effects of co-doping CeO_2 on refractive index and reflectivity from DFT calculation*, Comput. Mater. Sci. **158**, 197 (2019).

[25] W Bi, S Sun, S Bei, Y Jiang, *Effect of alloying elements on the mechanical properties of Mo_3Si*, Metals **11**, 1 (2021).

[26] R Lawler, J Cho, H C Ham, H Ju, S W Lee, J Y Kim, J Il Choi, S S Jang, *CeO_2(111) surface with oxygen vacancy for radical scavenging: A density functional theory approach*, J. Phys. Chem. C **124**, 20950 (2020).

[27] C Loschen, J Carrasco, K M Neyman, F Illas, *First-principles LDA + U and GGA + U study of cerium oxides: Dependence on the effective U parameter*, Phys. Rev. B **75**, 035115 (2007).

[28] N V Skorodumova, R Ahuja, S I Simak, I A Abrikosov, B Johansson, B I Lundqvist, *Electronic, bonding, and optical properties of CeO_2 and Ce_2O_3 from first principles*, Phys. Rev. B **64**, 1151081 (2001).

[29] Z N Jaf, Z T Jiang, H A Miran, M Altarawneh, *Thermo-elastic and optical properties of molybdenum nitride*, Can. J. Phys. **94**, 902 (2016).